

RESEARCH ARTICLE



# Enhancement of the oral bioavailability of isopropoxy benzene guanidine though complexation with hydroxypropyl- $\beta$ -cyclodextrin

Yixing Lu<sup>a,b</sup>, Liuye Yang<sup>a,b</sup>, Wanying Zhang<sup>a,b</sup>, Shiting Xie<sup>a,b</sup>, Feifei Zhao<sup>a,b</sup>, Xianfeng Peng<sup>c</sup>, Zonghua Qin<sup>c</sup>, Dongping Zeng<sup>a,b</sup> and Zhenling Zeng<sup>a,b</sup>

<sup>a</sup>Guangdong Provincial Key Laboratory of Veterinary Pharmaceutics Development and Safety Evaluation, National Risk Assessment Laboratory for Antimicrobial Resistance of Animal Original Bacteria, College of Veterinary Medicine, South China Agricultural University, Guangzhou, China; <sup>b</sup>Guangdong Laboratory for Lingnan Modern Agriculture, Guangzhou, China; <sup>c</sup>Guangzhou Insighter Biotechnology Co., Ltd, Guangzhou, China

## ABSTRACT

Isopropoxy benzene guanidine (IBG) is a novel substituted benzene guanidine analogue with antibacterial activity against multidrug-resistant bacteria. However, the bioavailability of IBG is not optimal due to its finite aqueous solubility, thus hampering its potential therapeutic exploitation. In this study, we prepared IBG/hydroxypropyl- $\beta$ -CD (IBG/HP- $\beta$ -CD) complex, and characterized it by differential scanning calorimetry, Fourier transform infrared spectroscopy, powder X-ray diffraction, and scanning electron microscopy. Physicochemical characterization indicated that the crystal morphology of IBG transformed into an amorphous state, thus forming IBG/HP- $\beta$ -CD inclusion complexes. Complexation with HP- $\beta$ -CD significantly improve the aqueous solubility, pharmaceutical properties, absorption, and bioavailability of IBG.

## ARTICLE HISTORY

Received 13 July 2022  
Revised 16 August 2022  
Accepted 21 August 2022

## KEYWORDS

Isopropoxy benzene guanidine; hydroxypropyl- $\beta$ -cyclodextrin; dissolution; bioavailability; pharmacokinetics

## 1. Introduction

Antibiotic resistance is a serious threat to public health (Ardal et al., 2020). ESKAPE pathogens (consisting of *Enterococcus faecium*, *Staphylococcus aureus*, *Klebsiella pneumoniae*, *Acinetobacter baumannii*, *Pseudomonas aeruginosa*, and *Enterobacter species*) are known for developing high levels of resistance to traditional antibiotic drugs, thus reducing treatment options for serious infections, and increasing mortality due to treatment failure (De Oliveira et al., 2020; Mancuso et al., 2021). In addition, these pathogens have shown resistance to first-line and last-resort antibiotics worldwide, leading to drug unavailability (Liu et al., 2016; He et al., 2019; Schwarz et al., 2021). Therefore, new agents and new ways to counter drug-resistant infections are urgently needed (McEwen & Collignon, 2018).

Given that guanidine has strong organic bases and a hydrophilic nature, guanidine compounds have been widely used in the treatment of various diseases and have become candidates for the further structural modification of new promising drugs (Sączewski & Balewski, 2013; Massimba-Dibama et al., 2015). Isopropoxy benzene guanidine (IBG), a new guanidine compound, which displayed potent bactericidal activity against multidrug-resistant *Enterococci* and clinical isolates of methicillin-resistant *Staphylococcus aureus* by targeting the cell membrane (Zhang et al., 2019, 2021). Furthermore, the combination of IBG and colistin has synergistic antibacterial effect on colistin-resistant

*Salmonella* (Kong et al., 2022). IBG is expected to become a new antibacterial agent in the treatment of bacterial infections. However, its bioavailability is not optimal due to its limited aqueous solubility.

Cyclodextrins (CDs) have greatly promoted the development of the pharmaceutical field (Shelley & Babu, 2018). CDs can overcome the low solubility of many drugs by complexing with the main active ingredient (Lakkakula & Macedo, 2014). HP- $\beta$ -CD has excellent inclusion properties for many compounds and shows only limited toxicity in animals and humans (Gould & Scott, 2005; Carneiro et al., 2019). Hu et al. prepared the inclusion complex of koumine (KME) with HP- $\beta$ -CD by solvent evaporation. KME/HP- $\beta$ -CD showed 52.34-fold greater solubility, enhanced absorption, and more than twofold greater relative bioavailability than KME (Hu et al., 2021). Li et al. prepared curcumin (CUR)/HP- $\beta$ -CD by a simple procedure of water-ethanol cosolvent incubation-lyophilization. Compared with that of CUR, the oral bioavailability of CUR/HP- $\beta$ -CD was boosted to 2.77-fold after intravenous administration in rats (Li et al., 2018). In addition, HP- $\beta$ -CD can be used in various medicinal products for oral, rectal, dermal, ophthalmic, and parenteral administrations, and is the safest among CD derivatives due to its inability to be absorbed through biological membranes (Irie & Uekama, 1997; Al-Heibshy et al., 2020; Manta et al., 2020).

This study aimed to encapsulate IBG into HP- $\beta$ -CD to enhance the solubility and bioavailability of IBG. IBG/HP- $\beta$ -CD was characterized by differential scanning calorimetry (DSC),

**CONTACT** Dongping Zeng ✉ [donytsang@scau.edu.cn](mailto:donytsang@scau.edu.cn); Zhenling Zeng ✉ [zllzeng@scau.edu.cn](mailto:zllzeng@scau.edu.cn) Guangdong Provincial Key Laboratory of Veterinary Pharmaceutics Development and Safety Evaluation, National Risk Assessment Laboratory for Antimicrobial Resistance of Animal Original Bacteria, College of Veterinary Medicine, South China Agricultural University, Guangzhou, 510642, China

© 2022 The Author(s). Published by Informa UK Limited, trading as Taylor & Francis Group.

This is an Open Access article distributed under the terms of the Creative Commons Attribution-NonCommercial License (<http://creativecommons.org/licenses/by-nc/4.0/>), which permits unrestricted non-commercial use, distribution, and reproduction in any medium, provided the original work is properly cited.

FT-IR spectroscopy (FT-IR), powder X-ray diffraction (PXRD), and scanning electron microscopy (SEM). Results confirmed that IBG was encapsulated into HP- $\beta$ -CD. The oral bioavailability of IBG and IBG/HP- $\beta$ -CD was evaluated in rats.

## 2. Materials and methods

### 2.1. Materials and instruments

Isopropoxy benzene guanidine (99.9%) was provided by Guangzhou Insighter Biotechnology (Guangzhou, China). HP- $\beta$ -CD was purchased from Shanghai Macklin Biochemical Co., Ltd (Lot:12087655). Thermal analyses were executed on DSC8000 (PE, USA). FTIR spectra were recorded on a Nicolet IS10 Fourier transform infrared spectrometer (Thermo Fisher), and PXRD spectra were recorded on an Ultima IV diffractometer (Rigaku, Japan). SEM images were recorded on a micro-surface morphology equipment (EVO MA 15, ZEISS, Germany). High-performance liquid chromatographic (HPLC) analysis was performed in a Shimadzu LC-20A system (Japan).

### 2.2. Phase solubility studies

Phase solubility studies were carried out following the method of Higuchi and Connors (Higuchi & Connors, 1965; Jansook et al., 2018). An excessive amount of IBG was added to 2 mL aqueous solutions of different HP- $\beta$ -CD concentrations (2, 4, 6, 8, 12, 16, and 24 mM). All samples were shaken at 25 °C and 100 rpm for 72 h until equilibrium was reached. After centrifugation, the supernatants were filtered through a 0.45  $\mu$ m membrane to remove undissolved IBG. The concentration of IBG in the HP- $\beta$ -CD solutions was determined by HPLC, and the analyses were performed in triplicate ( $n=3$ ). Apparent stability constant ( $K_s$ ) was calculated by the following equation (Nair et al., 2014; Pinto et al., 2020):  $K_s = \text{slope}/S_0(1 - \text{slope})$ , where  $S_0$  represents the intrinsic solubility of the drug, and the slope is the slope of the linear phase solubility diagram.

### 2.3. Preparation of IBG/HP- $\beta$ -CD

The required IBG and HP- $\beta$ -CD were weighed at a molar ratio of 1:3 to prepare the inclusion complex. HP- $\beta$ -CD was dissolved in distilled water at room temperature, followed by the slow addition of IBG solution in methanol. The solution was stirred at a certain speed at 50 °C for a few hours. The mixture was cooled to room temperature and freeze dried to obtain a white powdery IBG/HP- $\beta$ -CD. Physical mixtures were prepared by simply mixing IBG with HP- $\beta$ -CD.

### 2.4. Physicochemical characterization of the optimal IBG/HP- $\beta$ -CD inclusion complexes

#### 2.4.1. FT-IR spectroscopy

The FT-IR spectra of the KBr pellets of IBG, HP- $\beta$ -CD, physical mixtures, and inclusion complex of IBG with HP- $\beta$ -CD were obtained using a Nicolet IS10 Fourier transform infrared spectrometer. Data were acquired between 4000 and 500  $\text{cm}^{-1}$ .

#### 2.4.2. DSC

Thermal analyses of IBG, HP- $\beta$ -CD, physical mixtures, and inclusion complex were performed by differential scanning calorimetry (DSC8000, PE, USA). Sample was weighed (10 mg), placed in sealed aluminum pans, and scanned at 10 °C/min from 20 °C to 300 °C under flowing nitrogen gas. Thermograms were recorded.

#### 2.4.3. PXRD

PXRD analysis was performed at ambient temperature using an Ultima IV diffractometer (Rigaku, Japan) under Cu K $\alpha$  radiation ( $\lambda = 1.54056 \text{ \AA}$ , generator setting: 40 kV and 40 mA). Diffraction data were collected at the  $2\theta$  scanning range between 3° and 60° with a step size of 0.02° and a counting time of 2 s/step.

#### 2.4.4. SEM

The surface morphology of IBG, HP- $\beta$ -CD, mixture of IBG and HP- $\beta$ -CD, and inclusion complex of IBG with HP- $\beta$ -CD was studied using an EVO MA 15 (ZEISS, Germany) scanning electron microscope. The solid sample was mounted on aluminum stubs with double-sided carbon adhesive tape and then coated with gold for 30 min. Finally, SEM images were obtained at 10 kV to observe the surface morphology of the samples.

### 2.5. Determination of IBG content in the inclusion complex

The IBG content in IBG/HP- $\beta$ -CD was determined by HPLC ( $C_{18}$  column: 250 mm  $\times$  4.6 mm, 5  $\mu$ m; mobile phase: 0.1% phosphoric acid and acetonitrile in a ratio of 40:60; wavelength in UV detector: 323 nm). The standard curve of IBG (0.1–10  $\mu$ g/mL) was determined to be  $Y = 114376X + 8114.8$  ( $R^2 = 0.9997$ ; Y: absorption peak area; X: concentration).

The inclusion rate and yield of inclusion compound IBG were used to evaluate the inclusion effects of inclusion complexes and were calculated using the following formulas:

$$\text{Inclusion yield (\%)} = \left[ \frac{\text{IBG inclusion complex (mg)}}{\text{IBG (mg)} + \text{HP-}\beta\text{-CD (mg)}} \right] \times 100\%$$

$$\text{Inclusion ratio (\%)} = \left[ \frac{\text{IBG complex (mg)}}{\text{IBG (mg)}} \right] \times 100\%$$

### 2.6. Solubility of IBG and IBG/HP- $\beta$ -CD and in vitro release study

Excessive amounts of IBG and IBG/HP- $\beta$ -CD were added to distilled water to obtain a supersaturated solution (Hu et al., 2021). The samples were shaken at 37 °C for 24 h and 100 rpm. After centrifugation, the supernatants were filtered through a 0.22  $\mu$ m membrane and analyzed by HPLC.

### 2.7. Dissolution determination

Dissolution tests were performed using a USP apparatus 2 (paddle) with degassed deionized water (900 mL) as the

medium at  $37 \pm 0.3^\circ\text{C}$  with 100 rpm rotating speed. IBG (100 mg), inclusion complex (containing 100 mg of IBG), and mixture of IBG (100 mg) and HP- $\beta$ -CD (1200 mg) were used for the testing. The solution (5 mL) for each test was collected at 2, 5, 10, 15, 20, 30, 45, and 60 min. After each collection, 5 mL of isothermal medium was supplemented. The collected solution was filtered through 0.22 mm microporous membrane and analyzed by HPLC. Each test was repeated three times, and the dissolution rate was obtained from the standard regression curve equation.

### 2.8. In vivo pharmacokinetic studies

Based on reference and proper modification (Ding et al., 2020), SD rats ( $200 \pm 20$  g) were fasted for 12 h with free access to water before oral administration. The rats were divided randomly into two groups ( $n=6$ ) and received IBG or IBG/HP- $\beta$ -CD by oral gavage at a drug dose of 20 mg/kg. After drug administration, 0.5 mL of blood sample was collected at 0.08, 0.25, 0.5, 0.75, 1, 1.5, 2, 3, 4, 6, 8, 12, and 24 h. Each blood sample was centrifuged at 3000 r/min for 10 min at  $4^\circ\text{C}$ , and the supernatant was transferred to a centrifugal tube (2 mL). Afterward, 0.8 mL of 1% formic acid acetonitrile was added to 0.2 mL of plasma, followed by shaking for 1 min and centrifuging at 13,000 r/min for 10 min at  $4^\circ\text{C}$ . The supernatant was filtered with a  $0.22 \mu\text{m}$  filter for HPLC analysis. The values of IBG plasma PK parameters in single-dose PK studies were obtained by non-compartmental analysis in Phoenix WinNonlin<sup>®</sup> 5.2 (Certara, L.P., Princeton, NJ, USA).

## 3 Results and discussion

### 3.1. Phase solubility study

The phase solubility curve explains the complexation process and provides stoichiometry and  $K_s$  values for the inclusion complex (Pinto et al., 2020). The phase solubility curve of IBG and HP- $\beta$ -CD is shown in Figure 1. The water solubility of IBG increased linearly with the HP- $\beta$ -CD concentration in the range of 2–24 mM. The equilibrium solubility of IBG in water was  $0.33 \pm 0.03$  mg/mL. When the concentration of

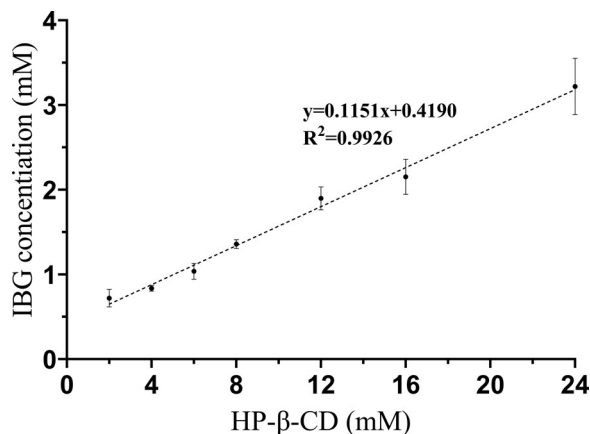


**Figure 1.** Phase solubility diagrams of IBG with different HP- $\beta$ -CD concentrations in distilled water at  $25 \pm 0.5^\circ\text{C}$  ( $n=3$ ).

HP- $\beta$ -CD was 24 mM, the solubility of IBG increased remarkably to 1.23 mg/mL (3.72-fold). According to the solubility diagrams by Higuchi and Connors, the phase solubility curve of IBG and HP- $\beta$ -CD is a typical AL-type curve. The regression coefficient ( $R^2$ ) exceeded 0.99, and the slope value (0.1151) was less than 1, indicating that the stoichiometry ratio of the IBG/HP- $\beta$ -CD system was 1:1. The  $K_s$  of IBG/HP- $\beta$ -CD was calculated according to the parameters of the phase solubility plot. The optimal values of  $K_s$  ranged  $50\text{--}2000 \text{ M}^{-1}$ , with small values indicate an extremely weak drug-CD interaction, and values above this range indicate that the drug is not fully released from the inclusion complex (Loftsson et al., 2005). In this study, the  $K_s$  of IBG/HP- $\beta$ -CD was calculated to be  $151.24 \text{ M}^{-1}$ , indicating a weak interaction between IBG and HP- $\beta$ -CD.

### 3.2. Preparation and optimization of IBG/HP- $\beta$ -CD inclusion complexes

During the process formation of an inclusion complex, the inclusion effect is significantly affected by the reaction temperature, stirring speed, and reaction time. HP- $\beta$ -CD was dissolved in distilled water, and the resulting mixture was stirred at a certain speed on a magnetic stirrer at a specific temperature. IBG solution in methanol was added slowly and stirred at a specified temperature for a particular time. The solution was stored in a refrigerator at  $-80^\circ\text{C}$  for 24 h and freeze dried for 48 h to obtain a white solid. The IBG inclusion complex was prepared under various conditions, such as the volume ratio of methanol and water from 1:9 to 3:7, different stirring speeds from 400 rpm to 600 rpm, various stirring temperatures from  $40^\circ\text{C}$  to  $60^\circ\text{C}$ , and stirring times from 2 h to 6 h. The IBG inclusion complex with the highest inclusion yield of 93.05% and the highest inclusion ratio of 80.45% was obtained under the following optimal condition: a 3:7 ratio of methanol and water, a stirring speed of 500 rpm, a reaction temperature of  $50^\circ\text{C}$ , and a reaction time of 4 h. Under these conditions, the resulted.

### 3.3. Physicochemical characterization of the optimal IBG/HP- $\beta$ -CD inclusion complexes

#### 3.3.1. SEM

The SEM images of IBG and its inclusion complex are presented in Figure 2. IBG showed prismatic crystals and compact structures (Figure 2(a)), and HP- $\beta$ -CD exhibited amorphous spherical particles (Figure 2(b)). The micrographs of physical mixtures exhibited a mixture of prismatic crystals and amorphous spherical particles (Figure 2(c)). IBG/HP- $\beta$ -CD displayed an amorphous sheet structure, and IBG was difficult to distinguish IBG from HP- $\beta$ -CD in the inclusion complexes (Figure 2(d)). These observations suggested that crystalline IBG may form a new solid phase complex in the cavity of HP- $\beta$ -CD.

#### 3.3.2. DSC

The DSC thermograms of the raw IBG, HP- $\beta$ -CD, physical mixtures, and IBG/HP- $\beta$ -CD are presented in Figure 3. The DSC thermogram of raw IBG showed a characteristic sharp

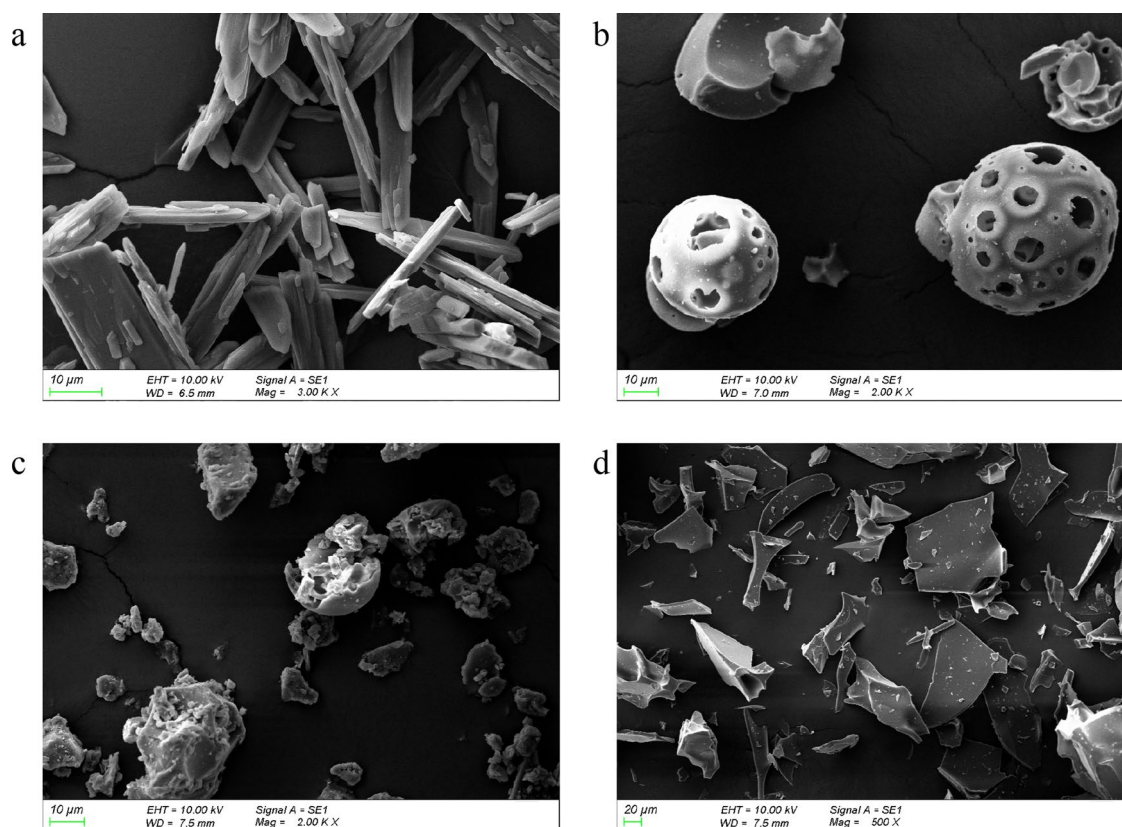


**Figure 2.** SEM images of raw IBG (a), HP-β-CD (b), physical mixtures (c), and IBG/HP-β-CD inclusion complexes (d).

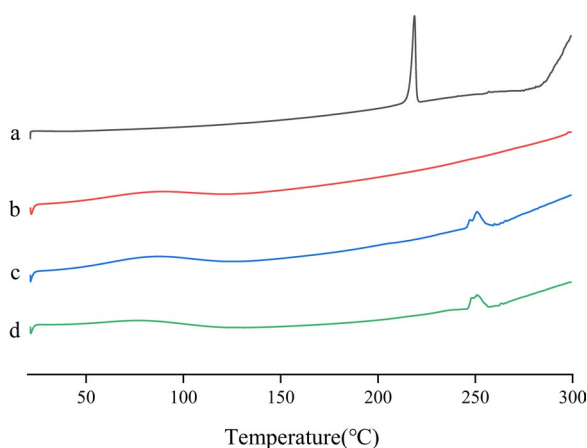


**Figure 3.** DSC curves of IBG (a), HP-β-CD (b), mixture of IBG and HP-β-CD (c), and IBG/HP-β-CD inclusion complexes (d).

endothermic peak at 218 °C indicating its crystallization state (Figure 3(a)). HP-β-CD did not show any endothermic peaks at 20–300 °C, indicating the absence of crystals (Figure 3(b)). The physical mixtures and IBG/HP-β-CD inclusion complexes showed an endothermic peak with reduced intensity and a slight change from the initial position compared with the bulk drug (Figures 3(c–d)). After the inclusion complex was formed, its endothermic peak completely disappeared in the thermogram, indicating that the IBG state was changed. The IBG molecules may have been embedded in the CD cavity, causing the crystalline drug to change to its amorphous properties (Hu et al., 2021).

### 3.3.3. PXRD

The PXRD results of IBG, HP-β-CD, physical mixtures, and IBG/HP-β-CD are shown in Figure 4. The spectrum of raw IBG exhibited a series of high-intensity peaks at 2θ values of approximately 5.31°, 21.17°, 22.53°, 23.33°, and 24.10° (Figure 4(a)), indicating its high crystallinity. The spectrum of HP-β-CD PXRD had no crystal peak, implying that it is essentially amorphous (Figure 4(b)). For the physical mixture, the PXRD spectrum still showed IBG corresponding to the peak intensity decrease (Figure 4(c)), suggesting that IBG still existed in the form of crystal. The PXRD pattern of IBG/HP-β-CD showed a broad hallow pattern similar to that of HP-β-CD, and the characteristic peak of raw IBG cannot be observed (Figure 4(d)). The results further confirmed that IBG/HP-β-CD was formed in an amorphous state.

### 3.3.4. FT-IR

The FT-IR spectra of raw IBG, HP-β-CD, physical mixtures, and IBG/HP-β-CD are shown in Figure 5. The peaks of IBG were found at 2975 (C–H stretching), 1652 (C=N stretching), 1509 (benzene skeleton vibration), and 1247 cm<sup>-1</sup> (C–O–C bond stretching vibrations) (Figure 5(a)). The broad absorption band of HP-β-CD at 3403 cm<sup>-1</sup> was attributed to the stretching vibration of the free OH group. Other peaks of HP-β-CD were found at 2929 (C–H bending), 1654 (H–O–H bending), 1157 (C–O stretching vibrations), and 1029 cm<sup>-1</sup> (C–O–C stretching vibrations) (Figure 5(b)). The characteristic absorption bands similar to those of IBG and HP-β-CD were also observed in the spectra of the physical mixtures (Figure 5(c)), indicating

the weak interaction between IBG and HP- $\beta$ -CD. The spectra of IBG/HP- $\beta$ -CD was highly similar to that of HP- $\beta$ -CD, and the characteristic absorptions peaks of IBG almost completely disappeared. This finding indicated that IBG was fully entrapped in the cavity of HP- $\beta$ -CD.

### 3.4. Solubility and in vitro release study

The water solubility of IBG, mixture of IBG and HP- $\beta$ -CD, and inclusion complex of IBG with HP- $\beta$ -CD was evaluated by preparing saturated solutions. The initial solubility of IBG was poor at  $0.33 \pm 0.03$  mg/mL, but significantly increased to  $54.18 \pm 1.57$  mg/mL after complexing with HP- $\beta$ -CD. The release profiles of IBG, physical mixtures, and inclusion complexes in deionized water are shown in Figure 6. The IBG release rate reached 5% within 1 h, and IBG/HP- $\beta$ -CD showed

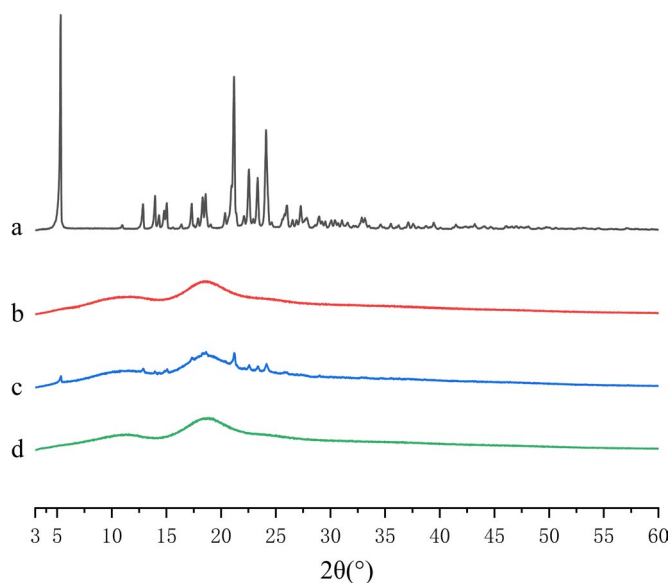


Figure 4. PXRD patterns of IBG (a), HP- $\beta$ -CD (b), mixture of IBG and HP- $\beta$ -CD (c), and IBG/HP- $\beta$ -CD inclusion complexes (d).

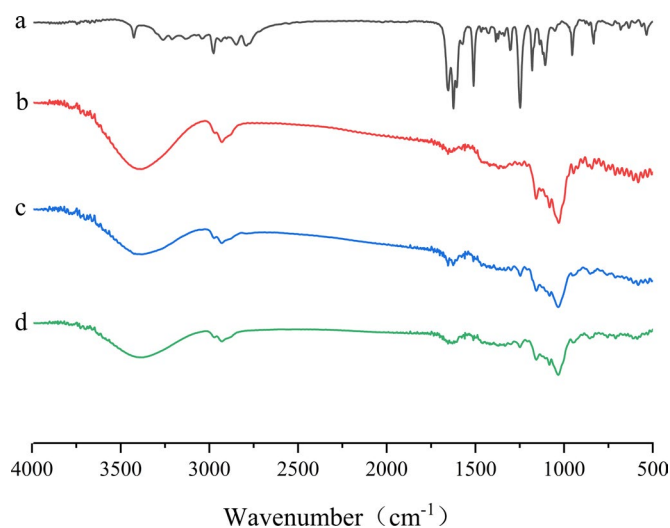


Figure 5. FT-IR spectra of IBG (a), HP- $\beta$ -CD (b), mixture of IBG and HP- $\beta$ -CD (c), and IBG/HP- $\beta$ -CD inclusion complexes (d).

a faster dissolution rate than IBG. The release rate approached 90% within 10 min and then plateaued.

### 3.5. In vivo pharmacokinetic study

To the best of our knowledge, this work is the first pharmacokinetic study of IBG *in vivo*. The mean plasma IBG concentration–time profiles following the oral administration of IBG and IBG/HP- $\beta$ -CD in rats are presented in Figure 7, and the main pharmacokinetic parameters are listed in Table 1. At almost all time points, the plasma concentration of IBG from IBG/HP- $\beta$ -CD was higher than that of raw IBG, indicating that the CD formulation could effectively enhance the plasma level of IBG. Compared with IBG suspension, IBG/HP- $\beta$ -CD greatly enhanced the  $C_{max}$  and  $AUC_{0-t}$  values after oral administration. Statistically, the  $C_{max}$  of IBG from IBG/HP- $\beta$ -CD was  $0.18 \pm 0.05$   $\mu$ g/mL, which was a significant (2.2-fold) improvement compared with that of the IBG suspension ( $0.08 \pm 0.01$   $\mu$ g/mL) ( $p < .01$ ). In particular, the  $AUC_{0-t}$  of IBG from IBG/HP- $\beta$ -CD complex ( $0.75 \pm 0.07$   $\mu$ g/mL·h) increased by 1.56-fold compared

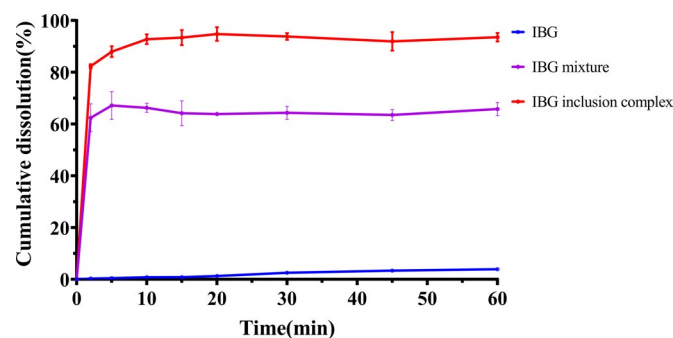


Figure 6. Dissolution curves of IBG, mixture of IBG and HP- $\beta$ -CD, and IBG/HP- $\beta$ -CD inclusion complex.

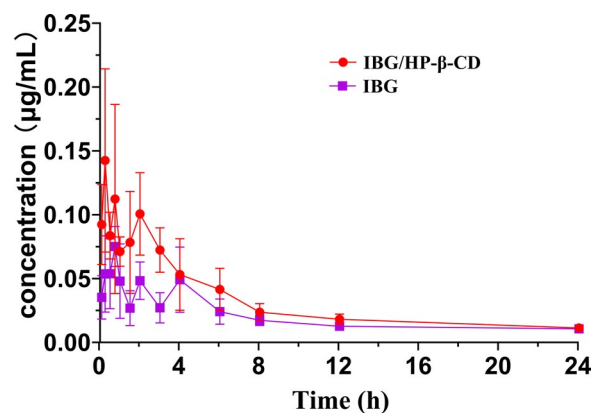


Figure 7. Mean plasma concentration–time curve following the oral administration of IBG and IBG/HP- $\beta$ -CD inclusion complexes in rats (mean  $\pm$  SD,  $n = 6$ ).

Table 1. Pharmacokinetic parameters of IBG and its inclusion complex.

Parameters	Unit	Value	
		IBG	IBG/HP- $\beta$ -CD
$T_{max}$	h	$0.67 \pm 0.24$	$0.46 \pm 0.22$
$C_{max}$	$\mu$ g/mL	$0.08 \pm 0.01$	$0.18 \pm 0.05^{**}$
$T_{1/2}$	h	$17.02 \pm 5.28$	$12.79 \pm 5.50$
$AUC_{0-t}$	$\mu$ g·h /mL	$0.48 \pm 0.06$	$0.75 \pm 0.07^{**}$

\*\* $p < .01$ , compared to IBG.

with that of the IBG suspension ( $0.48 \pm .06 \mu\text{g/mL}\cdot\text{h}$ ) ( $p < .01$ ), indicating that the oral bioavailability of IBG was increased by 1.56-fold due to its complexation with HP- $\beta$ -CD. The incremental bioavailability of IBG may be attributed to the increased solubility of IBG when incorporated in the inclusion complexes, allowing the drug to maintain its soluble form in the gastrointestinal tract (Wang et al., 2007; Shankar et al., 2021).

#### 4. Conclusion

In this study, we devised a reliable and consistent method to prepare an inclusion complex of IBG/HP- $\beta$ -CD with improved aqueous solubility (164-fold) compared with IBG itself. FTIR, DSC, PXRD, and SEM data indicated the successful formation of IBG/HP- $\beta$ -CD inclusion complexes. Pharmacokinetic evaluation of IBG/HP- $\beta$ -CD in rats showed that the pharmaceutical properties of absorption ( $C_{\text{max}}$ : .08 vs.  $0.18 \mu\text{g/mL}$ ) and bioavailability ( $0.48$  vs.  $0.75 \mu\text{g}\cdot\text{h/mL}$ ) of IBG were significantly improved. The results showed that IBG/HP- $\beta$ -CD can be used as an effective drug carrier to improve the solubility and bioavailability of IBG.

#### Acknowledgements

We thank Xinfang Chen, Jingyun Zhou from Instrumental Analysis & Research Center, South China Agricultural University for SEM sample processing and image acquisition.

#### Ethics statement

The animal study was reviewed and approved by Institutional Animal Care and Use Committee of South China Agricultural University (approval number: 2022b068).

#### Conflict of interest statement

Author XP and ZQ were employed by Guangzhou Insighter Biotechnology Co., Ltd. The remaining authors declare that the research was conducted in the absence of any commercial or financial relationships that could be construed as a potential conflict of interest.

#### Funding

This work was supported by Local Innovative and Research Teams Project of Guangdong Pearl River Talents Program (grant number 2019BT02N054).

#### References

Al-Heibshy F, Basaran E, Ozturk N, et al. (2020). Preparation and *in vitro* characterization of rosuvastatin calcium incorporated methyl beta cyclodextrin and Captisol((R)) inclusion complexes. *Drug Dev Ind Pharm* 46:1495–506.

Ardal C, Balasegaram M, Laxminarayan R, et al. (2020). Antibiotic development - economic, regulatory and societal challenges. *Nat Rev Microbiol* 18:267–74.

Carneiro SB, Costa DF, Heimfarth L, et al. (2019). Cyclodextrin (-) drug inclusion complexes: *In vivo* and *In vitro* approaches. *IJMS* 20:642.

De Oliveira D, Forde BM, Kidd TJ, et al. (2020). Antimicrobial resistance in ESKAPE pathogens. *Clin Microbiol Rev* 33:e00181–19.

Ding Y, Pang Y, Vara PC, et al. (2020). Formation of inclusion complex of enrofloxacin with 2-hydroxypropyl-beta-cyclodextrin. *Drug Deliv* 27:334–43.

Gould S, Scott RC. (2005). 2-Hydroxypropyl-beta-cyclodextrin (HP-beta-CD): a toxicology review. *Food Chem Toxicol* 43:1451–9.

He T, Wang R, Liu D, et al. (2019). Emergence of plasmid-mediated high-level tigecycline resistance genes in animals and humans. *Nat Microbiol* 4:1450–6.

Higuchi T, Connors KA. (1965). Phase-solubility techniques. In: C.N.R, ed., *Advances in analytical chemistry and instrumentation*. New York: Wiley-Interscience, 117–212.

Hu Q, Fu X, Su Y, et al. (2021). Enhanced oral bioavailability of koumine by complexation with hydroxypropyl-beta-cyclodextrin: preparation, optimization, *ex vivo* and *in vivo* characterization. *Drug Deliv* 28: 2415–26.

Irie T, Uekama K. (1997). Pharmaceutical applications of cyclodextrins. III. Toxicological issues and safety evaluation. *J Pharm Sci* 86:147–62.

Jansook P, Ogawa N, Loftsson T. (2018). Cyclodextrins: structure, physicochemical properties and pharmaceutical applications. *Int J Pharm* 535:272–84.

Kong L, Lu Y, Yang L, et al. (2022). Pharmacokinetics and pharmacodynamics of colistin combined with isopropoxy benzene guanidine against *mcr-1*-positive *Salmonella* in an intestinal infection model. *Front Microbiol* 13:907116.

Lakkakula JR, Macedo KR. (2014). A vision for cyclodextrin nanoparticles in drug delivery systems and pharmaceutical applications. *Nanomedicine (Lond)* 9:877–94.

Li N, Wang N, Wu T, et al. (2018). Preparation of curcumin-hydroxypropyl-beta-cyclodextrin inclusion complex by cosolvency-lyophilization procedure to enhance oral bioavailability of the drug. *Drug Dev Ind Pharm* 44:1966–74.

Liu YY, Wang Y, Walsh TR, et al. (2016). Emergence of plasmid-mediated colistin resistance mechanism MCR-1 in animals and human beings in China: a microbiological and molecular biological study. *Lancet Infect Dis* 16:161–8.

Loftsson T, Hreinsdóttir D, Másson M. (2005). Evaluation of cyclodextrin solubilization of drugs. *Int J Pharmaceut* 302:18–28.

Mancuso G, Midiri A, Gerace E, et al. (2021). Bacterial antibiotic resistance: the most critical pathogens. *Pathogens* 10:1310.

Manta K, Papakyriakopoulou P, Chountoules M, et al. (2020). Preparation and biophysical characterization of quercetin inclusion complexes with beta-cyclodextrin derivatives to be formulated as possible nose-to-brain quercetin delivery systems. *Mol Pharm* 17:4241–55.

Massimba-Dibama H, Mourer M, Constant P, et al. (2015). Guanidinium compounds with sub-micromolar activities against *Mycobacterium tuberculosis*. Synthesis, characterization and biological evaluations. *Bioorgan Med Chem* 23:5410–8.

McEwen SA, Collignon PJ. (2018). Antimicrobial resistance: a one health perspective. *Microbiol Spectr* 6:10–1128.

Nair AB, Attimaram M, Al-Dhubiab BE, et al. (2014). Enhanced oral bioavailability of acyclovir by inclusion complex using hydroxypropyl-beta-cyclodextrin. *Drug Deliv* 21:540–7.

Pinto L, Adeoye O, Thomasi SS, et al. (2020). Preparation and characterization of a synthetic curcumin analog inclusion complex and preliminary evaluation of *in vitro* antileishmanial activity. *Int J Pharm* 589:119764.

Sączewski F, Balewski Ł. (2013). Biological activities of guanidine compounds, 2008 - 2012 update. *Expert Opin Ther Pat* 23:965–95.

Schwarz S, Zhang W, Du X-D, et al. (2021). Mobile oxazolidinone resistance genes in Gram-positive and Gram-negative bacteria. *Clin Microbiol Rev* 34:e18820.

Shankar VK, Police A, Pandey P, et al. (2021). Optimization of sulfobutyl-ether-beta-cyclodextrin levels in oral formulations to enhance progesterone bioavailability. *Int J Pharm* 596:120212.

- Shelley H, Babu RJ. (2018). Role of cyclodextrins in nanoparticle-based drug delivery systems. *J Pharm Sci* 107:1741–53.
- Wang L, Jiang X, Xu W, et al. (2007). Complexation of tanshinone IIA with 2-hydroxypropyl-beta-cyclodextrin: effect on aqueous solubility, dissolution rate, and intestinal absorption behavior in rats. *Int J Pharm* 341:58–67.
- Zhang X, Han D, Pei P, et al. (2019). *In vitro* antibacterial activity of isopropoxy benzene guanidine against multidrug-resistant *Enterococci*. *Infect Drug Resist* 12:3943–53.
- Zhang X, Xiong W, Peng X, et al. (2021). Isopropoxy benzene guanidine kills *Staphylococcus aureus* without detectable resistance. *Front Microbiol* 12:633467.